

Tuning carrier concentration in a superacid treated MoS₂ monolayer

M. R. Molas,^{1,2,*} K. Gołasa,¹ Ł. Bala,^{1,2} K. Nogajewski,^{1,2} M. Bartos,² M. Potemski,^{1,2} and A. Babiński^{1,†}

¹*Institute of Experimental Physics, Faculty of Physics,
University of Warsaw, ul. Pasteura 5, 02-093 Warszawa, Poland*

²*Laboratoire National des Champs Magnétiques Intenses,
CNRS-UGA-UPS-INSA-EMFL, 25, avenue des Martyrs, 38042 Grenoble, France*

The effect of bis(trifluoromethane) sulfonimide (TFSI, superacid) treatment on the optical properties of MoS₂ monolayers is investigated by means of photoluminescence, reflectance contrast and Raman scattering spectroscopy employed in a broad temperature range. It is shown that when applied multiple times, the treatment results in progressive quenching of the trion emission/absorption and in the redshift of the neutral exciton emission/absorption associated with both the A and B excitonic resonances. Based on this evolution, a trion complex related to the B exciton in monolayer MoS₂ is unambiguously identified. A defect-related emission observed at low temperatures also disappears from the spectrum as a result of the treatment. Our observations are attributed to effective passivation of defects on the MoS₂ monolayer surface. The passivation reduces the carrier density, which in turn affects the out-of-plane electric field in the sample. The observed tuning of the carrier concentration strongly influences also the Raman scattering in the MoS₂ monolayer. An enhancement of Raman scattering at resonant excitation in the vicinity of the A neutral exciton is clearly seen for both the out-of-plane A₁' and in-plane E' modes. On the contrary, when the excitation is in resonance with a corresponding trion, the Raman scattering features become hardly visible. These results confirm the role of the excitonic charge state plays in the resonance effect of the excitation energy on the Raman scattering in transition metal dichalcogenides.

I. INTRODUCTION

Molybdenum disulfide (MoS₂) is the best known representative of semiconducting transition metal dichalcogenides (S-TMDs), which have recently attracted considerable attention due to their unique electronic structures and corresponding optical properties¹⁻⁴. Like other members of the S-TMD family, MoS₂ transforms from indirect- to direct-band-gap semiconductor when thinned down from the bulk form to the monolayer (ML) limit^{5,6}. As efficient light emitters, S-TMD monolayers are considered to be very promising building blocks of novel optoelectronic devices⁷⁻¹¹.

The potential of S-TMDs is related to their specific crystal structure which comprises strongly bound metal and chalcogen atoms arranged into one-molecule-thick single layers, which in N -layer crystals are stacked one on top of another and kept together by weak van der Waals interaction. In the ideal case of defect-free material, one of the features of such a structure is the absence of dangling bonds at the terminal chalcogen layers of each individual S-TMD monolayer. In practice, in order to profit from the unique properties of thin S-TMD films, it is absolutely crucial to take proper care of the quality and cleanliness of their surface. This means, in particular, keeping the surface free from chemical residues and avoiding defects which can negatively affect the desired optical properties of S-TMD layers. Recently, it has been reported that encapsulation of S-TMD monolayers in hexagonal boron nitride leads to suppression of the inhomogeneous contribution to the linewidths of excitonic resonances¹²⁻¹⁵. Another approach to heal the surface of N -layer S-TMDs is to subject them to a specific chemical treatment. Notably, Amani *et al.*¹⁶ have shown

that treating MoS₂ MLs with bis(trifluoromethane) sulfonimide (TFSI), referred to in what follows as a superacid, results in a considerable increase of the related photoluminescence (PL) intensity. The reported PL intensity growth amounts to about two orders of magnitude at room temperature. Subsequent works¹⁷⁻²¹ demonstrated that the room-temperature PL intensity of TFSI-passivated MoS₂ MLs grows by around one to three orders of magnitude in comparison with non-treated (as-exfoliated) MoS₂ samples. This suggests that the quality of source MoS₂ crystals used for exfoliation, determined by their origin (in the case of natural crystals), the growth procedure, the number of defects *etc.*, strongly influences the resultant effect of the superacid treatment. Moreover, it has been shown that the passivation of MoS₂ monolayers suppresses a dominant defect-related emission seen in their PL spectra measured at liquid helium temperature. However, the relative emission intensity due to the neutral and charged excitons seen at low temperature is not affected by the treatment process²⁰. In consequence, it can be expected that the results of the passivation process, *e.g.* the increase of the PL intensity, may strongly depend on initial sample's quality and/or experimental conditions.

In order to deepen the understanding of chemical processing effects on S-TMD monolayers, we have carried out a study of optical properties of ML MoS₂ subjected to the superacid treatment. We have not found any substantial increase in the room-temperature PL intensity caused by the passivation process. On the other hand, we have observed that the PL emission due to the negative trion quenches because of the treatment. A systematic energy redshift of the neutral excitons associated with both the A and B fundamental excitonic resonances at

the K points of the ML MoS₂ Brillouin zone (BZ) is also apparent in our results. We associate our observations with the passivation of unintentional doping centers at the surface of MoS₂ monolayer and the resulting decrease in the out-of-plane electric field's magnitude in the sample. The change of the excitonic energy affects also the Raman scattering (RS) efficiency in the studied MLs. A substantial enhancement of the RS intensity is observed when the excitation energy is resonant with the neutral exciton in the vicinity of the A resonance. On the contrary, the RS of light being in resonance with the corresponding trion can hardly be recognized in the recorded spectra.

II. SAMPLES AND EXPERIMENTAL SETUPS

MoS₂ monolayers were prepared by mechanical exfoliation of bulk crystals (2H phase) using a two-stage Scotch-tape- and polydimethylsiloxane-based technique²². After a non-deterministic transfer onto Si/(300 nm)SiO₂ substrates, the flakes of interest were first identified by visual inspection under an optical microscope and then cross-checked with Raman scattering and PL measurements at room temperature in order to unambiguously determine their thicknesses. The samples containing MoS₂ MLs were then chemically treated in bis(trifluoromethane) sulfonimide (TFSI) following the procedure described in Ref. 20. Several successive treatment rounds were applied to the same sample.

The PL and Raman scattering measurements were carried out using $\lambda=514.5$ nm (2.41 eV) and $\lambda=632.8$ nm (1.96 eV) lines of a continuous-wave Ar-ion and He-Ne laser, respectively. The studied samples were placed on a cold finger in a continuous flow cryostat mounted on xy motorized positioners. The excitation light was focused by means of a 50x long-working distance objective with a 0.5 numerical aperture giving a spot of about 1 μm diameter. The signal was collected via the same microscope objective, sent through a 0.5 m monochromator, and then detected using a liquid-nitrogen-cooled charge-coupled-device camera. The excitation power focused on the sample was kept at 50 μW during all measurements to avoid local heating. For RC study, the only difference in the experimental setup with respect to the one used for recording the PL and Raman scattering signals concerned the excitation source, which was replaced by a 100 W tungsten halogen lamp. The light from the lamp was coupled to a multimode fiber of a 50 μm core diameter, and then collimated and focused on the sample to a spot of about 4 μm diameter. We define the RC spectrum as $RC(E) = \frac{R(E) - R_0(E)}{R(E) + R_0(E)} \times 100\%$, where $R(E)$ and $R_0(E)$ are, respectively, the reflectances of the dielectric stack composed of an MoS₂ monolayer supported by an Si/SiO₂ substrate and of the Si/SiO₂ substrate alone.

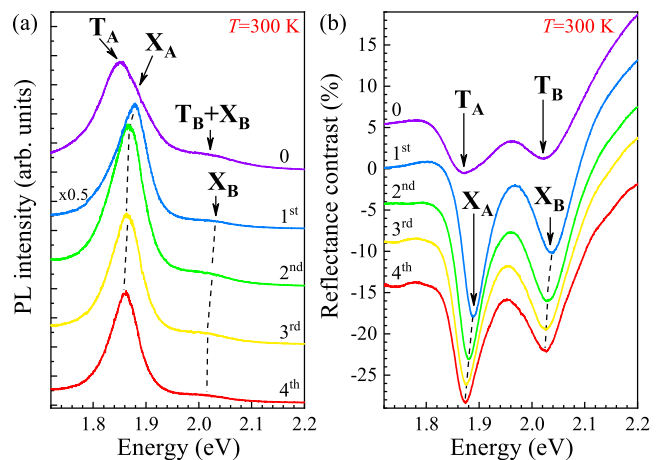


FIG. 1. Effect of successive TFSI passivations on (a) photoluminescence and (b) reflectance contrast spectra measured on a MoS₂ monolayer at room temperature. Denoted by '0' are the spectra recorded on an as-exfoliated ML, while labels '1st ... 4th' correspond to the number of passivations the ML was subjected to.

III. EXPERIMENTAL RESULTS

A. Carrier concentration in a superacid treated monolayer

Room-temperature ($T=300$ K) PL and RC spectra of an exfoliated MoS₂ monolayer before and after four successive TFSI passivations are presented in Fig. 1. A comparison between the PL spectra measured on the as-exfoliated ML and after the first round of superacid treatment allows us to identify up to three emission lines denoted by T_A , X_A and T_B+X_B (see Fig. 1(a)). We ascribe these peaks to the neutral (X_A , X_B) and charged (T_A and T_B) excitons formed in the vicinity of the so-called A and B excitonic transitions near the fundamental band gap at the K^\pm points of the BZ, which occur due to sizeable spin-orbit splitting in the valence band and smaller, though non-negligible, in the conduction band⁶. As can be appreciated in Fig. 1(a), the effect of superacid treatment on the PL spectrum is the most prominent after the first round. We observe a two-fold increase of the PL intensity as a consequence of the passivation, which stays in contrast to previous reports¹⁶⁻²⁰ demonstrating at room temperature an improvement of PL intensity by at least one order of magnitude. The second significant result of the first superacid treatment is a blueshift of the emission line related to the A exciton by about 30 meV. The corresponding RC spectrum of the as-exfoliated ML displays two resonance we denote by T_A and T_B in Fig. 1(b). After the first passivation, a similar blueshift of about 20 meV is also visible in

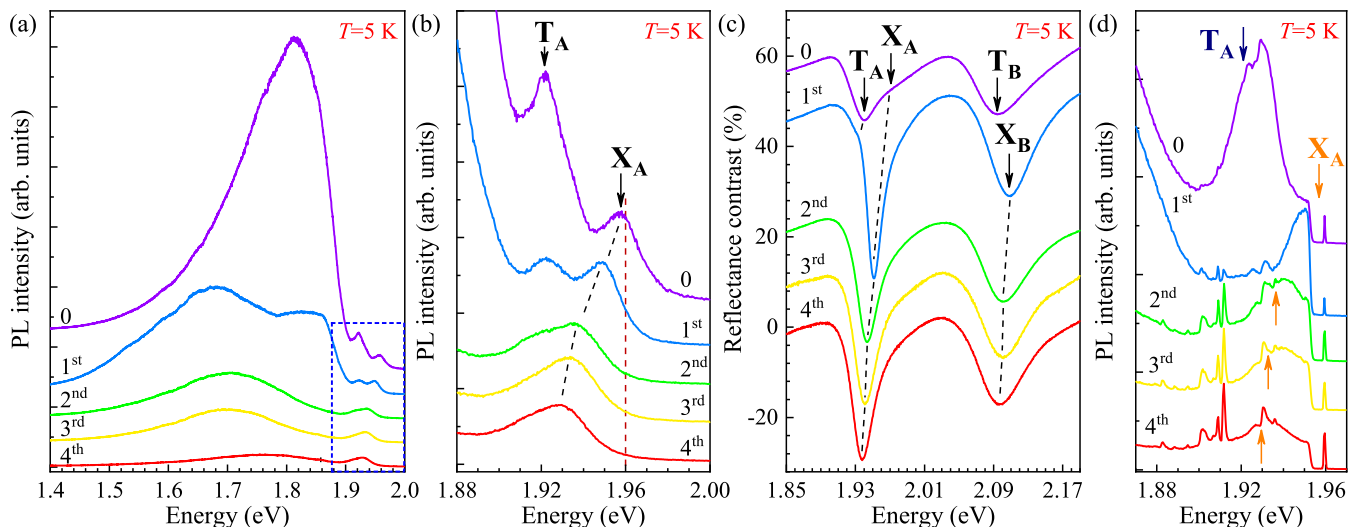


FIG. 2. Effect of successive TFSI passivations on low-temperature, $T=5$ K, (a),(b) photoluminescence, (c) reflectance contrast and (d) Raman scattering spectra measured on an MoS₂ monolayer at $\lambda=632.8$ nm excitation. Denoted by '0' are the spectra recorded on an as-exfoliated ML, while labels '1st ... 4th' correspond to the number of passivations the ML was subjected to. The red dashed vertical line in panel (b) indicates the energy of resonant Raman excitation conditions ($\lambda=632.8$ nm). The energies of T_A and X_A lines, inferred from the analysis of spectra shown in panel (b), are denoted by blue and orange arrows, respectively.

the RC spectra for both the A- (T_A , X_A) and B-exciton (T_B , X_B) resonances, and is accompanied by a gain in their intensities. Moreover, the blueshifts are followed by reduction of linewidths of the emission/absorption lines (see Figs 1(a) and (b)). The observed changes in both the PL and RC spectra as a result of the first superacid treatment can be understood in terms of a significant decrease of high non-intentional doping of the as-exfoliated monolayer. While mainly the charged excitons (T_A and T_B) contribute to both the PL and RC features in the as-exfoliated sample, the neutral excitons (X_A and X_B) dominate the PL and RC spectra after the first superacid treatment. In favour of our interpretation, the observed blueshifts of about 20-30 meV reasonably match the energy separation between the neutral and charged excitons (X_A and T_A) in monolayer MoS₂, reported to date in several publications^{20,23,24}. Moreover, it is well known that the oscillator strength of a neutral exciton is much bigger than that of a trion^{25,26}, which is reflected in the intensities of the corresponding resonances seen in the RC spectra plotted in Fig. 1(b) and Fig. 2(c). Note that an analogous effect is less visible for the B-exciton emission, probably due to its smaller intensity. The influence of successive passivations (starting from the second one) on the PL and RC spectra is less pronounced and mostly appears as monotonic redshifts of both the X_A and X_B resonances (the total shift amounts to about 10 meV after the fourth passivation round). This evolution can be explained in terms of modification of the built-in vertical electric field in the structure, *i.e.* the quantum-confined Stark effect, due to passivation of defects on the sample surface. Note that the linewidth of the A-exciton emis-

sion, see Fig. 1(a), is also reduced from ~ 90 meV before the superacid treatment to ~ 60 meV after the fourth passivation, which confirms the quenching of the trion emission and stays in agreement with similar results reported in Ref. 20.

The effect of superacid treatment described above can be studied in greater detail at low temperature because linewidths of excitonic emission/absorption resonances in S-TMDs significantly decrease with reducing the temperature²⁵⁻²⁷. Figure 2 presents a set of low-temperature ($T=5$ K) PL, RC and Raman scattering spectra measured on an MoS₂ ML before and after each of four successive passivations. As can be seen, both in the PL and RC spectra of the as-exfoliated ML, the X_A and T_A features are well resolved. This allows us to analyse the effect of superacid treatment more accurately. The PL spectrum of the as-exfoliated ML, shown in Fig. 2(a), is dominated by a broad emission band covering hundreds of meV's and commonly ascribed to defect states^{20,28}. An efficient quenching of this emission band with every successive passivation step is clearly visible. Its maximum intensity is on a comparable level as the X_A intensity after the fourth passivation. More information can be obtained by making a closer inspection of the low-temperature PL due to the A-transition-related excitonic features (see Fig. 2(b)). The observed peaks are attributed to the charged (T_A) and neutral (X_A) excitons. Similarly to the room-temperature behaviour (see Fig. 1(a)), as a result of the superacid treatment the PL signal coming from the trion complex quenches, leaving the neutral-exciton emission as a main feature of the spectrum. A systematic redshift of the X_A peak with successive treatment

rounds can also be noticed in Fig. 2(b). As we already proposed above, these two observations can be explained in terms of significant decrease of high non-intentional doping of the as-exfoliated monolayer, combined with a reduced influence of the quantum confined Stark effect reflecting the modification of the built-in vertical electric field in the structure due to passivation of defects on the sample surface. Both effects impact also the RC spectra in the energy range of the A and B excitons (see Fig. 2(c)). In particular, the observed non-monotonic evolution of the A-exciton minimum in the RC spectrum supports the discussed scenario. A substantial density of charge carriers in the as-exfoliated monolayer results in a strong trion T_A resonance which dominates the RC spectrum. Without any chemical treatment, the neutral exciton X_A can only be recognized as a high-energy component of the trion minimum. After the first passivation, the contribution from the trion can still be observed as a low-energy shoulder of the X_A dip, but further treatment rounds almost completely remove it from the spectrum. The reduction of the charge density and the evolution of the electric field in the sample also explain the behaviour of the RC minimum occurring in the B-exciton spectral range (see Fig. 2(c)), which is analogous to that corresponding to the A exciton. However, due to larger linewidths of the B-exciton resonances, it cannot be seen that clearly. In particular, the jump of the B-exciton dip to a higher energy after the first treatment round should share the same origin with an almost identical shift observed for the T_A+X_A feature. It means that the minimum in the RC spectrum corresponding to the B-resonance in the as-exfoliated ML is mostly composed of a contribution associated with the absorption of light by the charged exciton T_B . On the contrary, the RC features in the superacid-treated samples are due to the neutral excitons (X_B), which undergo a quantum confined Stark shift. It is worth to point out that the observed redshift resulting from the modification of the built-in vertical electric field in the ML is similar for both the X_A and X_B resonances and equals to 13 meV and 10 meV, respectively, as can be read from Fig. 2(b). Note that an analogous effect to described above can also be seen in the PL experiments for the emission lines in the vicinity of the A-resonance, X_A and T_A , presented in Fig. 2(a) and (b). In this case, however, the emission originating from the trion complex does not fully vanish from the PL spectra even after four passivations, probably due to a small residual doping which suffices to observe the trions in the photoluminescence, but not in absorption-like measurements.

One of pertinent questions regarding the results of optical experiments discussed above is the sign of the charged exciton resonances. In general, a trion, as a complex of an electron-hole pair and an extra carrier (electron or hole), can be negative (two electrons + a hole) or positive (an electron + two holes). In our case, an identification of which of these situations we are dealing with cannot be done in an unambiguous way. Unfortunately,

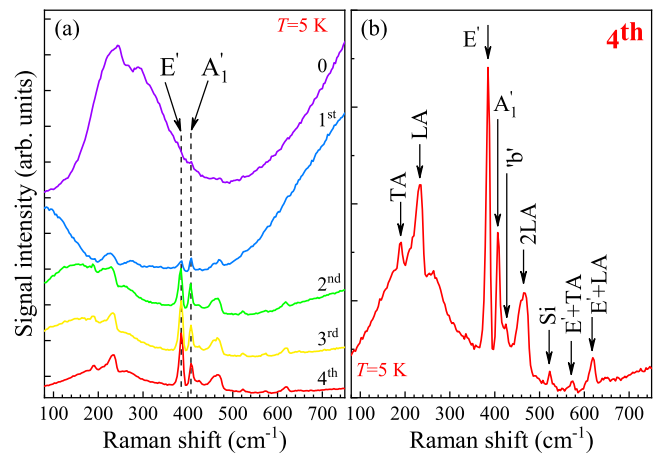


FIG. 3. (a) Effect of successive TFSI passivations on the Raman scattering spectrum measured under $\lambda = 632.8$ nm excitation on an MoS₂ monolayer at $T = 5$ K. Denoted by "0" is the spectrum recorded on an as-exfoliated ML, while labels '1st ... 4th' correspond to the number of passivations the ML was subjected to. (b) Low-temperature ($T = 5$ K) Raman scattering spectrum measured under $\lambda = 632.8$ nm excitation on an MoS₂ monolayer which underwent 4 superacid passivation rounds. Unless stated otherwise in the main text, the indicated phonons correspond to the M point of the Brillouin zone.

the same effects of the superacid treatment as observed in this work for the resonances in the vicinity of the A and B excitons might be expected for both negative and positive trions.

B. Resonant Raman scattering - the effect of the charge state

After four superacid treatment rounds, the X_A energy cumulatively downshifts by about 30 meV, see Fig. 2(d), becoming comparable to the T_A energy in the as-exfoliated MoS₂ ML. This evolution creates a unique opportunity to study Raman scattering under variable resonance conditions using a fixed excitation wavelength, in our case the $\lambda = 632.8$ nm line of a He-Ne laser, usually employed for this kind of investigations in MoS₂. It has previously been shown that excitation at this wavelength leads to resonant enhancement of the A_{1g} line in bulk MoS₂²⁹ and to multiphonon Raman scattering³⁰, both observed at low temperature. The effect of excitation energy on the optical response of ML MoS₂ was also studied^{31–34}, but the concept of carrying out such measurements under different resonant conditions varied by changing the carrier density in the ML has not been widely explored. Our work attempts to fill this gap.

The effect of superacid treatment on the low-temperature emission spectrum of ML MoS₂ excited with

$\lambda=632.8$ nm light is shown in Fig. 2(d). As indicated by orange arrows, such excitation energy matches the neutral exciton energy in the as-exfoliated sample. At lower energy an emission related to the T_A trion can be recognized as a structure superimposed on a broad peak centered at ~ 1.921 eV. As discussed earlier in the present paper, the trion disappears from the spectrum as a result of superacid treatment. This evolution of the spectrum shape is accompanied by a redshift of the neutral exciton. Moreover, with successive passivations, the structure due to Raman scattering becomes more and more visible. The spectra shown in Fig. 2(d), are also presented in Fig. 3(a) in a more conventional way, *i.e.* as a function of the Raman shift. The most intense Raman peaks in ML MoS₂ originate from two Raman-active modes: E' , which results from in-plane vibrations of the two S atoms with respect to the Mo atom, and A'_1 which is due to out-of-plane and out-of-phase vibrations of the S atoms³⁵. Surprisingly, the Raman scattering signal measured at $T=5$ K on the as-exfoliated monolayer is extremely weak, even though the excitation energy almost equals the X_A energy (see Fig. 2(c)). This leads to conditions under which the energies of the trion emission and of the first order Raman scattering processes coincide, or, in other words, come into resonance. When the monolayer is subjected to successive superacid treatments, the intensity of the Raman scattering signal significantly increases (for the A'_1 line, the enhancement amounts to about one order of magnitude). Another striking feature of the low-temperature spectra is the presence of an emission band at ~ 200 cm⁻¹, see Fig. 3(a). There are no center-zone Raman modes expected for ML MoS₂ in that energy range. The lineshape of the emission band corresponds, however, to the total integrated density of phonon states in the sample³⁶. This suggests that scattering involving single-phonon processes from outside the center of the BZ are allowed in this case. Two maxima, which are particularly well visible in the spectrum presented in Fig. 3(a), correspond to the transverse acoustic (TA) and longitudinal acoustic (LA) phonons near the M point from the border of the BZ. Most likely explanation of their presence in the Raman scattering spectrum points at disorder in the sample which localizes phonons^{37–39}. Such interpretation does not support, however, the substantial enhancement of the Raman peaks seen at low temperature in the spectra recorded on MoS₂ monolayers treated with superacid solution several times. The comparison between spectra measured on as-exfoliated sample with the trion- and defect-dominated emission and on the sample after four passivation rounds clearly suggests that the enhancement is associated with bringing the Raman features into resonance with the neutral exciton.

Another possibility to tune the resonance conditions for the Raman scattering is by varying sample's temperature. The temperature evolution of optical spectra mea-

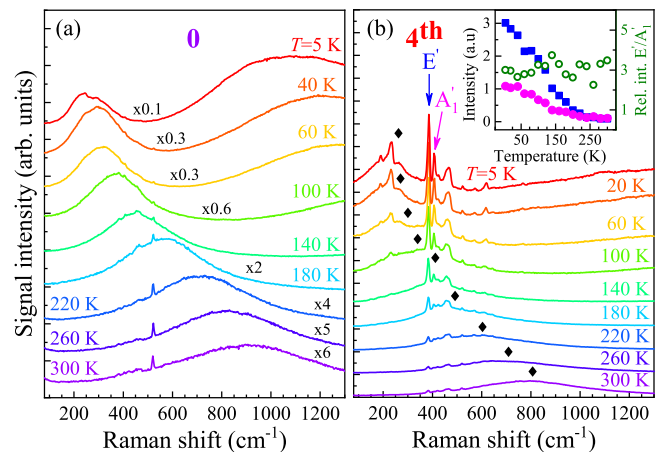


FIG. 4. Temperature evolution of resonant Raman scattering signal measured under $\lambda = 632.8$ nm excitation on an (a) as-exfoliated (0) and (b) four-times-passivated (4th) MoS₂ monolayer. The spectra in panel (a) are multiplied by the factors specified above the experimental curves. The black diamonds in panel (b) indicate the X_A energy inferred from the PL spectra measured under $\lambda = 514.5$ nm excitation. The temperature evolution of the E' and A'_1 modes intensities and their relative intensity are shown in the inset to panel (b).

sured on the as-exfoliated ML and after four passivations is presented in Fig. 4. As can be noticed in Fig. 4(b), the intensities of all Raman scattering peaks measured on the sample subjected to four treatment rounds gradually decrease with increasing temperature. We ascribe this effect to the shift of the neutral exciton energy away from the energy of the laser light due to the temperature dependence of the band gap^{25–27}. Surprisingly, the quenching affects both the A'_1 and E' modes. This is in contrast to the reported evolution of the Raman scattering efficiency in MoS₂ ML in which distinct exciton-phonon coupling strengths for the two modes can be explained by considering their symmetries with respect to the symmetries of the orbitals associated with the A, B and C (a high energy transition at around 2.7 eV) excitons³³. Our results show that at low temperature, the in-plane E' mode in ML MoS₂ undergoes a resonant enhancement despite the symmetry effect on the exciton-phonon interaction. Additional information can be gained from the analysis of the temperature-driven shift of the neutral exciton, X_A , energy. Its energy, as taken from the emission spectra excited at 514.5 nm, is denoted with diamonds in Fig. 4(b). No significant enhancement of the Raman-scattering-related emission spectra occurs for the outgoing resonance between the excitonic energy and the energy of scattered light. A monotonic decrease of the emission intensity is rather related to detuning the excitation laser energy off the neutral exciton energy. This may suggest a possible scenario responsible for the observed effects. At low temperature, the laser energy in use leads to the formation of neutral excitons at higher k-vectors, which then relax to the minimum energy state at the

K^\pm points by emitting discrete phonon modes (e.g. A_1'). With increasing temperature, the excitonic energy shifts away from the laser energy and the relaxation involves mainly acoustic phonons which do not contribute to the discrete emission spectrum observed at low temperature. As can be seen in Fig. 4(a), the process is not effective in a sample with high carrier density. In such a case, mostly acoustic phonons assist the relaxation processes and the discrete structure of the optical emission spectra can hardly be seen. Our observations point out the difference between the electron-phonon interactions with the neutral and charged excitons, as previously reported for monolayer WS_2 ⁴⁰. Furthermore, we showed that the carrier concentration in the studied MoS_2 monolayer plays a significant role for the intensity of the resonant Raman scattering signal. It is clear that our qualitative explanation should be supported by more strict theoretical analysis which is beyond the scope of this experimental work. We do believe, however, that our results can contribute to the understanding of fundamental physical processes in S-TMDs, which is of prime interest for their potential applications.

IV. CONCLUSIONS

In conclusion, we have studied the effect of superacid (TFSI) treatment on the optical properties of monolayer MoS_2 with the aid of photoluminescence, reflectance con-

trast and Raman scattering spectroscopy employed in a broad temperature range. We have observed that the defect-related low-energy photoluminescence progressively disappears from the spectrum as a result of successive TFSI passivations. Moreover, we have found that the treatment results in systematic quenching of the charged exciton emission/absorption and the redshift of the neutral exciton emission/absorption associated with both the A and B resonance transitions at the K^\pm points of the monolayer MoS_2 BZ. Furthermore, our results demonstrate that the charge state of dominant excitons in ML MoS_2 affects the Raman scattering under resonant excitation conditions. In particular, it has been shown that much more effective scattering occurs for the resonance with the neutral exciton than with the trion.

ACKNOWLEDGEMENTS

The work has been supported by the European Research Council (MOMB project no. 320590), the EC Graphene Flagship project (no. 604391), the National Science Center (grants no. DEC-2013/11/N/ST3/04067, DEC-2015/16/T/ST3/00496, UMO-2017/24/C/ST3/00119, UMO-2017/27/B/ST3/00205), the Nanofab facility of the Institut Néel, CNRS UGA, and the ATOMOPTO project (TEAM programme of the Foundation for Polish Science co-financed by the EU within the ERDFund).

* maciej.molas@fuw.edu.pl

† adam.babinski@fuw.edu.pl

¹ K. S. Novoselov, D. Jiang, F. Schedin, T. J. Booth, V. V. Khotkevich, S. V. Morozov, and A. K. Geim, *Proc. Natl. Acad. Sci. U. S. A.* **102**, 10451 (2005).

² Q. H. Wang, K.-Z. Kourosch, A. Kis, J. N. Coleman, and M. S. Strano, *Nat. Nanotechnol.* **7**, 699 (2012).

³ M. Koperski, M. R. Molas, A. Arora, K. Nogajewski, A. Slobodeniuk, C. Faugeras, and M. Potemski, *Nanophotonics* **6**, 1289 (2017).

⁴ G. Wang, A. Chernikov, M. M. Glazov, T. F. Heinz, X. Marie, T. Amand, and B. Urbaszek, *Rev. Mod. Phys.* **90**, 021001 (2018).

⁵ K. F. Mak, C. Lee, J. Hone, J. Shan, and T. F. Heinz, *Phys. Rev. Lett.* **105**, 136805 (2010).

⁶ A. Splendiani, L. Sun, Y. Zhang, T. Li, J. Kim, C.-Y. Chim, G. Galli, and F. Wang, *Nano Letters* **10**, 1271 (2010).

⁷ Z. Yin, H. Li, H. Li, L. Jiang, Y. Shi, Y. Sun, G. Lu, Q. Zhang, X. Chen, and H. Zhang, *ACS Nano* **6**, 74 (2012).

⁸ B. W. H. Baugher, H. O. H. Churchill, Y. Yang, and P. Jarillo-Herrero, *Nature Nanotechnology* **9**, 262 (2014).

⁹ J. S. Ross, P. Klement, A. M. Jones, N. J. Ghimire, J. Yan, D. G. Mandrus, T. Taniguchi, K. Watanabe, K. Kitamura, W. Yao, D. H. Cobden, and X. Xu, *Nature Nanotechnology* **9**, 268 (2014).

¹⁰ F. Withers, O. Del Pozo-Zamudio, A. Mishchenko, A. P. Rooney, A. Gholinia, K. Watanabe, T. Taniguchi, S. J. Haigh, A. K. Geim, A. I. Tartakovskii, and K. S. Novoselov, *Nat. Mater.* **14**, 301 (2015).

¹¹ J. Binder, F. Withers, M. R. Molas, C. Faugeras, K. Nogajewski, K. Watanabe, T. Taniguchi, A. Kozikov, A. K. Geim, K. S. Novoselov, and M. Potemski, *Nano Letters* **17**, 1425 (2017).

¹² F. Cadiz, E. Courtade, C. Robert, G. Wang, Y. Shen, H. Cai, T. Taniguchi, K. Watanabe, H. Carrere, D. Lagarde, M. Manca, T. Amand, P. Renucci, S. Tongay, X. Marie, and B. Urbaszek, *Phys. Rev. X* **7**, 021026 (2017).

¹³ J. Wierzbowski, J. Klein, F. Sigger, C. Straubinger, M. Kremser, T. Taniguchi, K. Watanabe, U. Wurstbauer, A. W. Holleitner, M. Kaniber, K. Müller, and J. J. Finley, *Scientific Reports* **7**, 12383 (2017).

¹⁴ G. Wang, C. Robert, M. M. Glazov, F. Cadiz, E. Courtade, T. Amand, D. Lagarde, T. Taniguchi, K. Watanabe, B. Urbaszek, and X. Marie, *Phys. Rev. Lett.* **119**, 047401 (2017).

¹⁵ D. Vaclavkova, J. Wyzula, K. Nogajewski, M. Bartos, A. O. Slobodeniuk, C. Faugeras, M. Potemski, and M. R. Molas, *Nanotechnology* **29**, 325705 (2018).

¹⁶ M. Amani, D.-H. Lien, D. Kiriya, J. Xiao, A. Azcatl, J. Noh, S. R. Madhupathy, R. Addou, S. KC, M. Dubey, K. Cho, R. M. Wallace, S.-C. Lee, J.-H. He, J. W. Ager, X. Zhang, E. Yablonovitch, and A. Javey,

- Science* **350**, 1065 (2015).
- ¹⁷ M. Amani, P. Taheri, R. Addou, G. H. Ahn, D. Kiriya, D.-H. Lien, J. W. Ager, R. M. Wallace, and A. Javey, *Nano Letters* **16**, 2786 (2016).
 - ¹⁸ M. Amani, R. A. Burke, X. Ji, P. Zhao, D.-H. Lien, P. Taheri, G. H. Ahn, D. Kiriya, J. W. Ager, E. Yablonovitch, J. Kong, M. Dubey, and A. Javey, *ACS Nano* **10**, 6535 (2016).
 - ¹⁹ H. Kim, D.-H. Lien, M. Amani, J. W. Ager, and A. Javey, *ACS Nano* **11**, 5179 (2017).
 - ²⁰ F. Cadiz, S. Tricard, M. Gay, D. Lagarde, G. Wang, C. Robert, P. Renucci, B. Urbaszek, and X. Marie, *Applied Physics Letters* **108**, 251106 (2016).
 - ²¹ D. Kiriya, Y. Hijikata, J. Pirillo, R. Kitaura, A. Murai, A. Ashida, T. Yoshimura, and N. Fujimura, *Langmuir* **34**, 10243 (2018).
 - ²² A. Castellanos-Gomez, M. Buscema, R. Molenaar, V. Singh, L. Janssen, H. S. J. van der Zant, and G. A. Steele, *2D Materials* **1**, 011002 (2014).
 - ²³ K. F. Mak, K. He, C. Lee, G. H. Lee, J. Hone, T. F. Hein, and J. Shan, *Nat. Mater.* **12**, 207 (2013).
 - ²⁴ F. Cadiz, C. Robert, G. Wang, W. Kong, X. Fan, M. Blei, D. Lagarde, M. Gay, M. Manca, T. Taniguchi, K. Watanabe, T. Amand, X. Marie, P. Renucci, S. Tongay, and B. Urbaszek, *2D Materials* **3**, 045008 (2016).
 - ²⁵ A. Arora, M. Koperski, K. Nogajewski, J. Marcus, C. Faugeras, and M. Potemski, *Nanoscale* **7**, 10421 (2015).
 - ²⁶ M. R. Molas, K. Nogajewski, A. O. Slobodeniuk, J. Binder, M. Bartos, and M. Potemski, *Nanoscale* **9**, 13128 (2017).
 - ²⁷ A. Arora, K. Nogajewski, M. Molas, M. Koperski, and M. Potemski, *Nanoscale* **7**, 20769 (2015).
 - ²⁸ M. R. Molas, C. Faugeras, A. O. Slobodeniuk, K. Nogajewski, M. Bartos, D. M. Basko, and M. Potemski, *2D Materials* **4**, 021003 (2017).
 - ²⁹ G. L. Frey, R. Tenne, M. J. Matthews, M. S. Dresselhaus, and G. Dresselhaus, *Phys. Rev. B* **60**, 2883 (1999).
 - ³⁰ K. Gołasa, M. Grzeszczyk, P. Leszczyński, C. Faugeras, A. A. L. Nicolet, A. Wyszmołek, M. Potemski, and A. Babiński, *Applied Physics Letters* **104**, 092106 (2014).
 - ³¹ Y. Lee, S. Park, H. Kim, G. H. Han, Y. H. Lee, and J. Kim, *Nanoscale* **7**, 11909 (2015).
 - ³² M. Placidi, M. Dimitrievska, V. Izquierdo-Roca, X. Fontané, A. Castellanos-Gomez, A. Pérez-Tomás, N. Mestres, M. Espindola-Rodriguez, S. López-Marino, M. Neuschitzer, V. Bermudez, A. Yaremko, and A. Pérez-Rodríguez, *2D Materials* **2**, 035006 (2015).
 - ³³ B. R. Carvalho, L. M. Malard, J. M. Alves, C. Fantini, and M. A. Pimenta, *Phys. Rev. Lett.* **114**, 136403 (2015).
 - ³⁴ J. Kutrowska-Girzycka, J. Jadczyk, and L. Bryja, *Solid State Communications* **275**, 25 (2018).
 - ³⁵ C. Lee, H. Yan, L. E. Brus, T. F. Heinz, J. Hone, and S. Ryu, *ACS Nano* **4**, 2695 (2010).
 - ³⁶ A. Molina-Sánchez and L. Wirtz, *Phys. Rev. B* **84**, 155413 (2011).
 - ³⁷ K. Gołasa, M. Grzeszczyk, K. P. Korona, R. Bożek, J. Binder, J. Szczytko, A. Wyszmołek, and A. Babiński, *Acta Physica Polonica A* **124**, 849 (2013).
 - ³⁸ K. Gołasa, M. Grzeszczyk, J. Binder, R. Bożek, A. Wyszmołek, and A. Babiński, *AIP Advances* **5**, 077120 (2015).
 - ³⁹ S. Mignuzzi, A. J. Pollard, N. Bonini, B. Brennan, I. S. Gilmore, M. A. Pimenta, D. Richards, and D. Roy, *Phys. Rev. B* **91**, 195411 (2015).
 - ⁴⁰ M. R. Molas, K. Nogajewski, M. Potemski, and A. Babiński, *Scientific Reports* **7**, 5036 (2017).